



On Numerical Investigation of Semi-empirical Relations Representing Local Nusselt Number at Lower Nozzle-target Spacing's

S. Mohd Umair^{*a}, N. P. Gulhane^b, A. R. A. Al-Robaian^c, S. A. Khan^d

^a MPSTME – NMIMS University, India

^b Veermata Jijabai Technological Institute, Mumbai, India

^c Qassim University, Saudi

^d Mechanical Engineering Department, Faculty of Engg., IIUM, Kuala Lumpur, Malaysia

PAPER INFO

Paper history:

Received 21 November 2018

Received in revised form 19 December 2018

Accepted 03 January 2019

Keywords:

Local Nusselt Number

Prandtl Number

Nozzel

Numerical Simulation

Heat Sink

Gamma-theta Model

ABSTRACT

Examining the cooling rate using impingement of air jet finds a wide application in electronic packaging and micro-scale fluid heat interaction systems, While the prediction of Nusselt profile at low nozzle-target spacing is a big issue. The plot of area average Nusselt number magnitude against the nozzle-target spacing (Z/d) shows a gradual decrement in the profile upto $Z/d = 1$ and beyond that is steady. The present work aims in anticipating the profile of Nusselt number using semi-empirical relations. These semi-empirical relations are derived using regression analysis which is carried out between Re , Z/d and local Nusselt number. The data required for regression are obtained through computation. Numerical simulations are accomplished for different impinging and geometric parameters. The semi-empirical power law relations are correlated between Z/d and Re . These are predicted differently for four distinct region of heat sink (stagnant point, near jet region, far jet region, near wall region). The developed correlations are found to bear negative exponent with Z/d and positive exponent with Re . The negative power of r/d and Z/d varies from 0.23 – 0.64 and 0.0025 – 0.38, respectively, While the exponents of Re varies in the positive range of 0.4-0.76.

doi: 10.5829/ije.2019.32.01a.18

NOMENCLATURE

Q	Heat flux (w/m^2)	Z	Nozzle target spacing (m)
K	Thermal conductivity ($w/m-k$)	Re	Reynolds number
ΔT	Temperature difference ($^{\circ}C$)	Cond	Conduction
t	Thickness (m)	Conv	convection
h	Heat transfer Coefficient (w/m^2-k)	rad	Radiation
d,D	Diameters of nozzle (m)	Greek Symbols	
v	Velocity of jet (m/s)	ρ	Density (kg/m^3)
A,p,q	Regression constants	ϵ	Emissivity
r	Radial distance (m)	σ	Stefan-Boltzmann constant ($Wm^{-2}k^{-4}$)
Nu	Nusselt number	γ	Gamma model
b	Base plate	θ	Theta model
a	Ambient condition		

1. INTRODUCTION

The demanding challenges in electronic packaging system and various material processing industries have

given a paramount task to the research area of localized cooling technology. Generally, a characterized cooling rate in such systems is achieved by impinging a well confined air jet. The cooling in electronic packaging system has recently demanded the practice of non-uniform cooling rate. The non-uniformity in the cooling

*Corresponding Author Email: umair.siddique@nmims.edu (S. Mohd Umair)

rate is achieved by generating huge velocity gradient at the target side. The study of non-uniformity achieved in the cooling is of great significance. The trend of studying the cooling rate through flat plate and pin fin heat sink has started since 1980. Up-till date and during the intervening time, most of the works are focused on experimental study. The present study focuses over the determination of local Nusselt magnitude in the Nusselt profile, which is generated at low nozzle-target spacing. It is well known that when jet is impinging on the surface and the free jets exhausted to the atmosphere will have different flow field and the pressure energy associated with them.

1. 1. Literature Overview Katti and Prabhu [1] examined the local Nusselt distribution over a 0.05mm steel foil under a constant heat flux. The impinging Re varies from 12000 to 28000. The work has completely discussed the semi-empirical relations for local Nu value. Here, the semi-empirical relations are defined separately on either side of $Z/d = 4$. Not only this, the regions formed over the target surface were classified as stagnation region, near jet region, far jet region and near wall region [1]. Alimohammadi et al. [2] numerically plotted the Nusselt profile for wide range of nozzle-target spacing and impinging Reynolds number. The secondary peaks are observed initially at low Z/d . Alimohammadi et al. [2] successfully gave the semi-empirical relation for stagnant point Nusselt number in terms of impinging Reynolds number and nozzle-target spacing. Also the article suggested the use of Shear Stress Transport (SST) + Gamma-theta model for running the simulations in commercial CFX solver. Gorji et al. [3] examined various types of turbulence models in determining the flow profile. SST model proves well in capturing the heat transfer delay in transition region. Hence, with use of other turbulence model the temperature profile seems to be inaccurately plotted. Robin and Florain [4] concluded, the exact augmentation of coolingrate by invoking Gamma Theta turbulence model along with SST. This incorporates the effect of intermediacy and instant changeover of Reynolds magnitude.

Paul et al. [5] numerically validated, the combine effect of Gamma-Theta turbulence model along with SST on flow behavior and corresponding Nusselt number. The study of flow profile was carried out over the flat plat and airfoil geometry, also the onset transition regions were far accurately captured when compared with experimental results.

Angioletti et al. [6] observed the stagnation zone of flow profile by impinging air jet over heat sink numerically and compared the velocity contours with that recorded through PIV. Far appreciable agreement was reported using SST + Gamma-Theta model.

Hung et al. [7] experimentally calculated the heat impedance for different heat sink at different impinging

and geometric parameters. Wide range of dependency on these parameters where observed on the Nusselt profile.

Hani and Suresh [8] came up with the concept of area average heat transfer rate for pinned and unpinned surface by calculating the area under the Nusselt profile curve. 60% enhancement in cooling rate for the use of pinned surface was observed. Semi-empirical relation for area average Nusselt number was proposed as $Nu = 3.361 Re^{0.724} Pr^{0.4} (De/d)^{-0.689} (S/d)^{-0.10}$.

Suresh and Vincent [9] came up with local Nusselt number concept. Experiments were carried out for different impingement and geometric parameters. Also the use of multi-jet was incorporated. Large variation in local Nusselt profile in form of secondary peaks were observed. According to Suresh and Vincent [9] correlation representing the cooling rate for stagnant point is given as $Nus = 0.161 Re^{0.707} Pr^{0.4} (H/d)^{-0.104}$.

From the previous survey it is well understood that the study of area average Nusselt profile and Local Nusselt profile are done enormously. Also the study of secondary peak is done to quite a large extend. But the numerical study with validation of experimental results lags. Also the study of different contours in analyzing the physical effect behind the occurrence of abnormality in Nusselt profile lags. Chougle et al. [10] came forward and analyzed the velocity and pressure contour of heat sink under the impingement of air jet and gave the physical significance of occurrence of transition region for the abnormal secondary rise.

Luis and Suresh [11] came up with the comparison of single and multiple jet nozzle impingement over the bare and modified heat sink. The conclusion for the optimum nozzle-target spacing and penetrating momentum was concluded. Luis and Suresh [11] tried to get the optimum nozzle target spacing and impinging Reynolds number for maximum heat transfer, but failed to do so.

Umair and Gulhane [12] examined the occurrence of secondary peak in the Nusselt profile by varying Re and Z/d . The ratio of Re and Z/d was treated as a non-dimensional number in examining the occurrence of secondary peaks. Above 6000 value of this constant the secondary peak in the Nusselt curve arises. For evaluating the Nusselt profile Umair and Gulhane [13] considered a 2-D axi-symmetric geometric model with appropriate boundary conditions for simulating purpose [12]. The simulation is carried out in commercial CFX solver by the use of SST + Gamma-theta turbulence model. Whereas Umair and Gulhane [13] investigated the consequence of target surface material in inducing the non-uniformity in Nusselt profile. Here, pseudo Prandtl number of heat sink was subjected to variation and different Nusselt profile was recorder at $Z/d = 4$ and $Re = 10000$. The cause behind the rises in the average

Nusselt magnitude with decrease in thermal diffusivity was the abnormal distribution of heat flow in the target surface [13]. The grid size use in the study consist of two critical length having edge division of 550 by 400 [12, 13]. SST + Gamma-theta were the corresponding turbulence model used for numerical simulations [13]. Not only this Umair and Gulhane carried out the numerical study over pin fin heat sink [14]. Here, the grid independence study, turbulence modeling, turbulence intensity and turbulence Prandtl number study was reported [14]. No doubt, the implementation of SST + Gamma-theta proved to capture the best results.

Khameneh et al. [15] reported an accurate prediction of single phase laminar flow in micro-channel using Fluent solver. Also the forced convection heat transfer was accurately predicted. Here the physics of area average Nusselt number was of great concerned. Sundaram and Venkatesan [16] analyzed the flow field over the pin fin surface using RNG turbulence model and reported an error of 0.3% in the evaluation of average temperature. On the other hand, Khoshhravan and Soleimani [17] reported the interaction of radiation and conduction rate of heat transfer on natural convection. The distribution of local Nusselt magnitude was found to be far effected due to the radiation heat loss. The novelty of this paper lies in determining the local Nusselt magnitude when the nozzle-target spacing is below the critical value. The critical value is the one below which Nusselt profile shows drastic increment with the decrease in its value. After studying the above survey and looking into the research gap, the authors of the present paper concludes the existences of research gap in determination of Nusselt number magnitude in empirical form for lower value of nozzle-target spacing.

1. 2. Objectives The present work work aims in determining the semi-empirical relation representing local Nu number magnitude. These empirical relations are determined in terms of nozzle target spacing, Reynolds number and non-dimensional radial distance. These are the functional Pi terms present in semi-empirical relations. The computational simulations are achieved by solving the 3-D axis symmetric geometry in the commercial CFX solver. The semi-empirical relations are determined separately for $r/d = 0$ (stagnant region), $r/d < 1$ (near jet region), $1 < r/d < 2.5$ (far jet region) and $r/d > 2.5$ (near wall region).

2. EXPERIMENTAL STUDY

The current experimental setup is designed to generate the temperature profile across the flat plate by impinging air jet (Figure 1). The experimental setup consists of inlet nozzle, plenum, blower, by pass



Figure 1. Photograph of experimental setup

facility, variable heat flux input and heat sink. The nozzle is 16mm in diameter and length of 105mm which confines the air jet and generates a velocity profile which impinges on the heat sink. The heat sink consists in form of flat plate (100mm × 100mm) for the current setup and is provided with constant heat flux input (1500W/m²). All though the value of heat input doesn't play any significant role in altering the value of Nusselt number, as stated by Katti and Prabhu [1]. The inlet blower carrying capacity of 0.5 m³/s forces the atmospheric air into the plenum, which carries many open tubes. This helps in streamlining the air and reduce the consequence of turbulence intensity on the developed Nusselt profile.

Here the radiation component of heat loss at 50⁰C of steady temperature for base plate rounds to 8.39 W/m² (Equation (2.3)). Since an aluminum sheet is used as a target surface, the corresponding emissivity is selected as 0.032 for the present calculation [1]. However the heat loss due to the radiation and natural convection from the back surface is not considered, since the back side of the target surface is exposed to constant heat flux input (1500 W/m²). Still, Katti and Prabhu [1] estimated these components of back side loss and concluded a very less magnitude. However for the present work, the magnitude of radiation loss in comparison with the supplied heat input (1500 W/m²) approximates to 0.01%. Looking into the conduction component of heat loss, the geometric thickness (t) which happens to be in the denominator of Equation (2.2) possesses a very less magnitude. This may boost up the conduction heat lost. But the magnitude (ΔT) which represents the temperature difference between the top and bottom surface of target heat sink is examined to be very small. This is due to the low value of geometric thickness possessed by the target surface. No doubt, the corresponding heat lost due to conduction approximates to 33.4 W/m² (Calculated using Equation (2.2)). Hence, around 2.2% of heat loss occurs due to conduction from

side wall. This is a very small in comparison with the supply heat input (1500W/m^2). 5 K type thermocouple radial mounted below the plate carrying the precision of $\pm 0.1^\circ\text{C}$ and measuring range between $0 - 400^\circ\text{C}$. The readings of thermocouples are recorded using data logger system. Since the position of thermocouples are fixed, hence a decreasing nature temperature profile is observed.

Energy balance equations are as followings:

$$Q = Q_{cond} + Q_{conv} + Q_{rad} \quad (2.1)$$

$$Q_{cond} = K \left(\frac{\Delta T}{t} \right) \quad (2.2)$$

$$Q_{rad} = \varepsilon \sigma (T_b^4 - T_a^4) \quad (2.3)$$

As per the calculation, the approximated radiation component of heat loss is found to be 8.39 Watts per square meter (Equation (2.3)), Whereas the heat loss due radiation from back surface rounds to 0.01% [1]. Since, the temperature gradient across the thickness of heat sink is very small, the conduction rate of heat lost from the plate can be neglected. Hence, the overall cooling rate due to convection dominates. Also, the time required for achieving the steady temperature profile over the plate is too large, hence computational simulations are recommended for the present setup

2. 1. Measurement of Cooling Rate The overall cooling rate due to conduction is calculated using Equation (2.4), while the non-dimensional Nusselt number representing the magnitude of cooling rate is calculated using Equation (2.5).

$$h = \frac{Q}{A \times (T_b - T_a)} \quad (2.4)$$

$$Nu = h \times \frac{d}{k_a} \quad (2.5)$$

Uncertainties in the measurement of heat transfer coefficients are carried out using the method suggested by Moffat [18] and are around 3.4% and 2.9%, respectively, at Reynolds number of 12,000 and 28,000.

Whereas the uncertainty recorded due to variation in heat flux input is negligible as reported by katti and Prabhu [1].

2. 2. Computational Methodology In the Present work, numerical simulation using ANSYS CFX solver [12–14] is done by importing the grid independent geometry from the commercial mesh design modeler. Umair and Gulhane has massively published the article based on the numerical modelling [13–15], hence the grid independence test is not repeated in the present

work. However, the mesh size used for simulation is defined in the later part of the work. The commercial CFX solver is based on the continuity and naiver-stoke model along with a flow model. The equation and its relevance is widely discussed in the previous article of Umair and Gulhane [13-15].

2. 3. Computational Domain, Turbulance Model and Optimum Grid Size

The present work simulates a 3-D model as shown in Figure 2. This model is rotated by 1 deg along Z – axis in order to fulfil the three dimensional concept of solver. A constant velocity input is given to the input of nozzle which in turn generates a velocity profile at the exit. The opening wall of the domains to atmosphere are treated as adiabatic wall, while the bottom surface of flat plate given a constant heat flux input.

The length L1 is defined as a symmetry line. Here, spacing between nozzle and target (Z/d) and the radial length of the heat sink are marked L1 and L2 respectively, since the grid independence study is of great concerned with these distances. During the process of simulation, the bottom face of the target surface is provided with constant heat flux (1500W/m^2), while the exit of nozzle is given the velocity inlet (Figure 3) [12–14]. The opening of the computational domains is set to atmospheric pressure [12–14]. Actually the structuring of the computational domain is extensively carried out by the same authors in the previous publications. Hence, emphasizing on the selection of turbulence model and grid independent geometry is not necessary for the present paper. Umair and Gulhane [12–14] have investigated the flow behavior and heat transfer phenomenon using different turbulence model. The aggregate solution of heat transfer using SST + Gamma–theta model has proved to capture the most accurate value. Based on the extensive study carried out by Umair and Gulhane [12–14], the present work implements the SST + Gamma-Theta model, in order to predict the exact Nusselt profile.

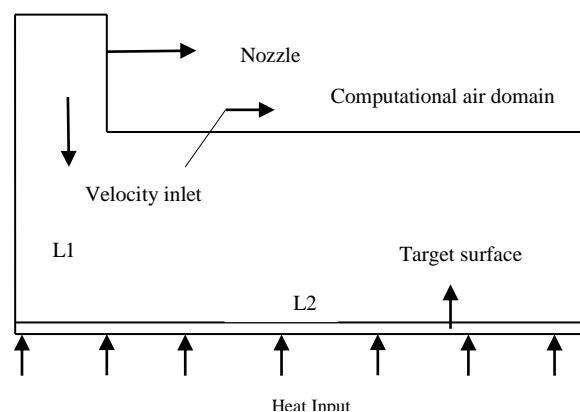


Figure 2. Layout of three dimensional computational domain

Not only has this, Umair and Gulhane [12–14] carried the grid independence study of the same computational domain (Figure 3). Umair and Gulhane [12–14] recommended the use of grid size which accommodates 550 divisions on L1 and 400 divisions on L2 (provided $Z/d = 4$) with the growth rate of 1.08 and 1.03 respectively to be the most optimum grid in accurately predicting the Nusselt profile. To maintain orthogonality, tetrahedral mesh is used in the current study. In order to optimize the computational cost, the far wall regions are adopted with coarse mesh with a sufficient magnitude of y^+ distance [12–14]. Also, it is suggested to alter the division over the edges L1 by keeping the growth rate constant, if Z/d is subjected to variation. Looking into the previous study [12–14], the present work doesn't demonstrate the grid independence and turbulence modeling study. The geometric model with 550 and 400 number of edges over L1 and L2 is selected with a growth rate of 1.08 and 1.03. SST + Gamma-theta model is used for the simulations.

Also, the present computational domain is compared with experimental results carried out at $Z/d = 2 - 4$ and Re ranging from 5000 to 10000. Quite good agreement of numerical work with experimental work is observed. The difference in the numerical and experimental result arises due to itemedianacy and onset transition of Reynolds number. This is not weakly predicted using numerical model.

The designed geometry is further imported into the commercial mesh modeler (ANSYS CFX), where the domains are subjected to fine grids size. Generally tetrahedral meshing with appropriate number of divisions over the critical edges (L1, L2) and flexibility in growth rate is being materialized for the present geometry. Also the number of divisions over the critical edges can be varied as and when the geometry is subjected to the change in size.

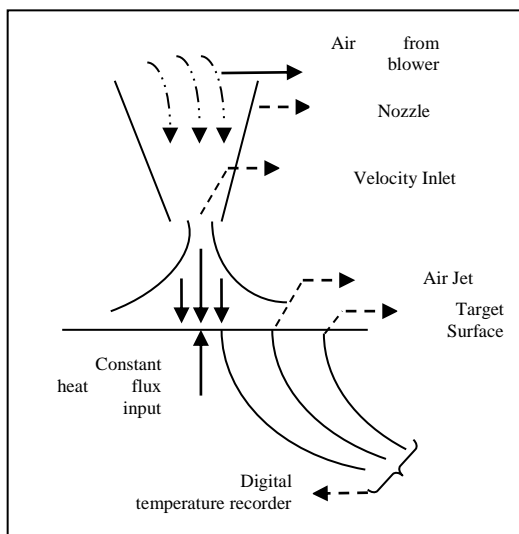


Figure 3. Schematic layout of experimental setup

Hence it is recommended to alter the number of divisions as and when the computational geometry is subjected to the change in geometric parameters (Z/d). However the grid independency in the present case is done for $Z/d = 4$. During the process of meshing, the edges containing air jet and base plate are intentionally divided into more number of division as compared to the other edges (Figure 4).

Figure 5 and 6 shows the validation of numerical model with experimental results at $Z/d = 2 - 4$ and $Re = 5000 - 10000$. On the other hand Figure 7 shows the validation of numerical results with ethat experimentally reported by Katti and Prabhu [1].

2. 4. Computational Ranges of Different Parameters

The computational of Z/d varies from 2 – 4, as below and above this value the parameter doesn't plays any significant effect in disturbing the Nusselt profile. On the otherhand the value of Re is ranging from 5000-15000, above 15000 the turbulence model needs more time for computation in order to predict the adverse pressure gradient and onset transition of Reynolds number. This is shown in Table 1.

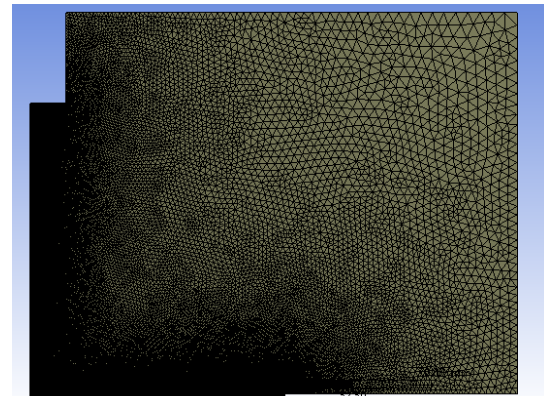


Figure 4. Schematic diagram of grid

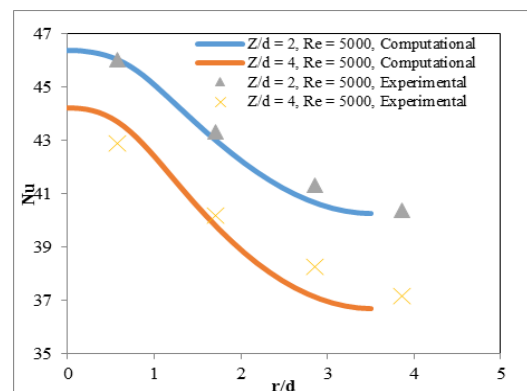


Figure 5. Comparison of experimental and computational Nusselt profiles at $Re = 5000$ and $Z/d = 2$ and 4

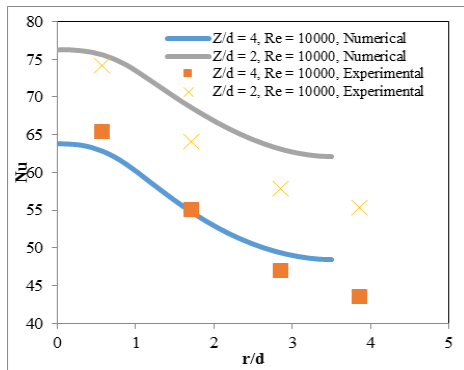


Figure 6. Comparison of experimental and computational Nusselt profiles at Re = 10000 and Z/d = 2 and 4

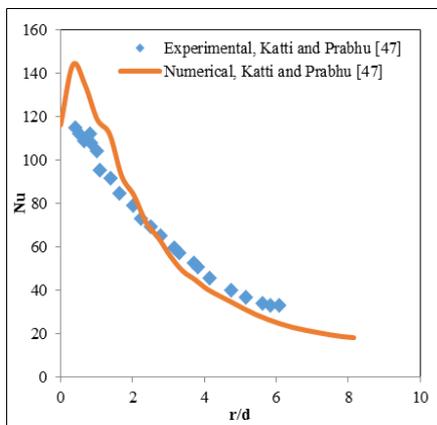


Figure 7. Comparison of computational Nusselt profile with experimental one, reported by Katti and Prabhu [1] at Re = 12000 and Z/d = 4

TABLE 1. Ranges of different parameters

Parameters	Range
Velocity of impinging jet	5 m/s – 15 m/s
Nozzle-Target spacing (Z/d)	2 – 6
Diameter of nozzle	16 mm
Area of base plate	100 mm× 100 mm
Heat input	15 Watts
Thickness of base plate	0.05 mm – 1mm

3. RESULTS AND DISCUSSION

Nusselt profiles can be easily predicted using a commercial solver, but the prediction of local Nusselt values in terms of functional parameter becomes an issue. The semi-empirical relation in the present work is defined between the Nusselt number and functional Pi terms. The functional Pi terms are Reynolds number (Re) and nozzle-target spacing (Z/d) (Equations (3.1), and (3.2)). Also the semi-empirical relation reported through regression analysis is given by Equation (3.3)

$$Pi_1 = \frac{Z}{d} \tag{3.1}$$

$$Pi_2(Re) = \frac{\rho V D}{\mu} \tag{3.2}$$

$$Nu = A \times (Pi_1)^p \times (Pi_2)^q \tag{3.3}$$

In order to determine the constants A, p, q regression analysis performed for Nu between Z/d and Re. For the purpose of regression, Z/d ranges between 0.1 -1 (with difference of 0.1) while the individual nozzle-target spacing is subjected to a variation in Reynolds number of 10000, 20000, 30000, 40000 and 50000. It is not feasible to reported the Nusselt profile for every Reynolds number, however the present work reports the Nusselt profile for Re = 10000. As seen from Figure 8, for less Z/d the Nusselt profile elevates and resembles small secondary rise. Also the nature of profile is gradually decreasing and meets at r/d = 2.5, this is the point of relaminarisation. Hence, the semi-empirical relations are proposed separately for different regions over the target surface (r/d = 0 (stagnant region), r/d<1 (near jet region), 1 < r/d < 2.5 (far jet region), r/d > 2.5 (far wall region)). However, the area average Nusselt profile against Z/d can be reported for different Reynolds number (Figure 9). It is very clear from Figure 9, the area average Nusselt number decreases with increase in Z/d. This is valid for lower Z/d's (Z/d <1), whereas above Z/d = 1 the area average Nusselt value almost remains independent of it. The present work is totally inclined towards the determination of local Nu value at lower Z/d (Z/d<1). Also an elevation in the profile is observed for increasing Re value.

3. 1. Semiempirical Relations The functional representation of semi-empirical equation for different range of r/d is shown in the Table 2.

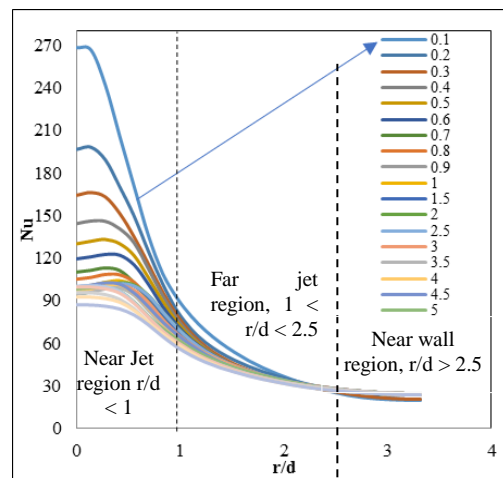


Figure 8. Nusselt profiles at Re = 10000 and Z/d = 0.1-1.5

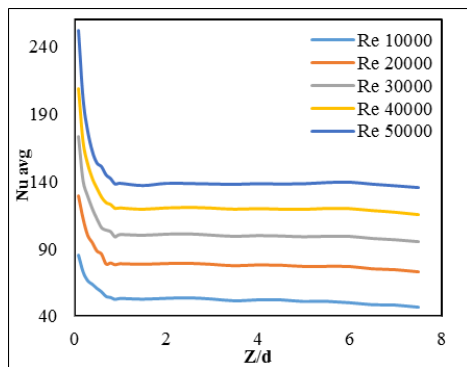


Figure 9. Area average Nusselt profile versus Z/d

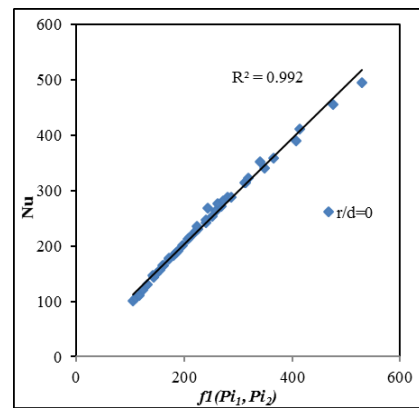


Figure 10. Best curve fit for Nu versus $f_1(Pi_1, Pi_2)$

TABLE 2. Functional representation of semi-empirical relations for different ranges of r/d

r/d	Semiempirical functions
r/d=0	$f_1(Pi_1, Pi_2)$
r/d < 1	$f_2(Pi_1, Pi_2)$
1 < r/d < 2.5	$f_3(Pi_1, Pi_2)$
r/d > 2.5	$f_4(Pi_1, Pi_2)$

The result of regression yields the value of constants A, p, q for different range of r/d. Regression is performed between Nu, r/d, Z/d and Re. The semi-empirical relations are tabulated against the corresponding functional parameter in Table 3. Also Figures 10, 11, 12 and 13 represents the graphical plot of $f_1(Pi_1, Pi_2)$, $f_2(Pi_1, Pi_2)$, $f_3(Pi_1, Pi_2)$ and $f_4(Pi_1, Pi_2)$ against the local Nu value respectively.

As shown in Table 3, r/d is inversely proportional to local Nu number and the magnitude of negative power varies from -0.23 to -0.64. This implies that with increase in the r/d value from stagnation region the negative power also increases.

Also, Z/d carries a negative power ranging from -0.38 to 0.162 for r/d < 2.5, but for r/d > 2.5, Z/d carries a positive power magnitude of 0.0025. On the other hand, Re carries a positive power relation with local Nu magnitude and the power ranges from 0.482 – 0.66 for different ranges of r/d.

TABLE 3. Semi-empirical relations for different ranges of r/d

r/d	Functional representation	Semi-empirical relation
r/d=0	$f_1(Pi_1, Pi_2)$	$Nu = 1.2(Z/d)^{-0.38} (Re)^{0.482}$
r/d < 1	$f_2(Pi_1, Pi_2)$	$Nu = 0.713(r/d)^{-0.23} (Z/d)^{-0.12} (Re)^{0.52}$
1 < r/d < 2.5	$f_3(Pi_1, Pi_2)$	$Nu = 0.45(r/d)^{-0.86} (Z/d)^{-0.162} (Re)^{0.768}$
r/d > 2.5	$f_4(Pi_1, Pi_2)$	$Nu = 0.113(r/d)^{-0.64} (Z/d)^{0.0025} (Re)^{0.66}$

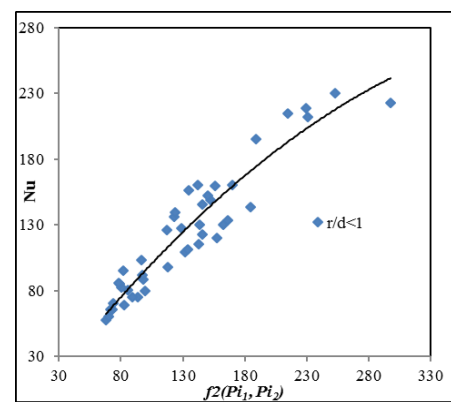


Figure 11. Best curve fit for Nu versus $f_2(Pi_1, Pi_2)$

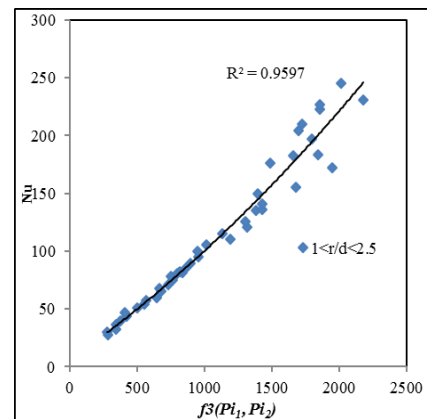


Figure 12. Best curve fit for Nu versus $f_3(Pi_1, Pi_2)$

In order to draw a feasible conclusion relating the power of different parameter, a complication of powers of different parameters is presented in Table 4. Also in order to predict the flow behaviour the present work also reports the plot of velocity contour at Z/d = 4 and Re = 10000. Also the work takes an initiative in reporting the velocity development across nozzle-target spacing, hence a contour of velocity in air is shown in Figure 14.

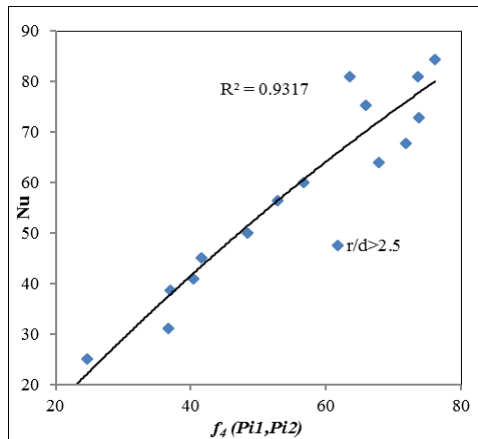


Figure 13. Best curve fit for Nu versus $f_d(Pi_1, Pi_2)$

TABLE 4. Power of different functional parameters (Pi terms) present in semi-empirical relations

r/d	A	Power of r/d	P (Z/d)	Q (Re)
r/d = 0	1.2	0	-0.38	0.482
r/d < 1	0.713	-0.23	-0.12	0.52
1 < r/d < 2.5	0.45	-0.86	-0.162	0.768
r/d > 2.5	-0.64	-0.64	0.0025	0.66

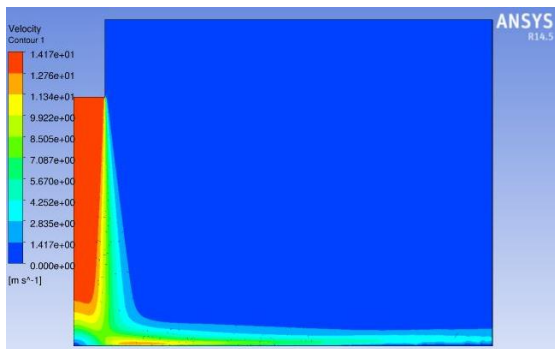


Figure 14. Velocity contour at $Z/d = 4$ and $Re = 10000$

4. CONCLUSION

The outline of the present work lies in numerically computing the Nusselt profile for different ranges of parameter using turbulence model in CFX solver. Since the research gap of the present work lies in predicting the Nusselt profile at lower Z/d . Hence, the key objective of the present work lies in determination of semi-empirical relations which is stated in Table 3. In order to discuss the magnitude of dependency of various functional parameters, the powers are summarized in Table 4. The inverse variation of r/d with the Nusselt number magnitude justifies the gradual decrement of Nusselt profile as the radial increases away from the stagnant point. The power magnitude of r/d initially

increases in the negative co-ordinate from -0.23 to -0.86. This is because of the gradient in cross velocity magnitude over the heat sink. The increase of negative power takes place in near jet ($r/d < 1$) and far jet region ($1 < r/d < 2.5$), while the magnitude of the exponent decreases as the Nusselt profile approach the near wall region ($r/d > 2.5$). This intermediate decrease in the exponent magnitude occurs due to re-laminarization in the flow field. As far as Z/d is concerned, the negative power variation with the Nusselt magnitude justifies the increase in the developing flow length decreases the local Nusselt number magnitude. This physics is applicable only for $Z/d < 1$. At lower Z/d the impinging air generates more turbulence which results in the enhancement of heat transfer rate. This enhancement in heat rate is comparatively more as than that achieved due to relaxation in developing flow length (Z/d). Above all, the Nusselt magnitude carries a positive variation with the power of Re. The magnitude of this power increases with the radial distance away from stagnant point. Magnitude of the power is the least at stagnant region, since the generation of back flow and swirl restricts some heat transfer. The power magnitude increases with the radial distance, since the velocity gradient occurring after the stagnant point plays a vital role in trapping the air flow in contact with the target plate. On behalf of this, the contact magnitude of air is more in near jet, far jet and near wall region; hence the heat flow rate is dominant from these regions as far as the impinging Reynolds number is concerned.

5. REFERENCES

- Katti, V. and Prabhu, S., "Experimental study and theoretical analysis of local heat transfer distribution between smooth flat surface and impinging air jet from a circular straight pipe nozzle", *International Journal of Heat and Mass Transfer*, Vol. 51, No. 17-18, (2008), 4480-4495.
- Alimohammadi, S., Murray, D.B. and Persoons, T., "Experimental validation of a computational fluid dynamics methodology for transitional flow heat transfer characteristics of a steady impinging jet", *Journal of Heat Transfer*, Vol. 136, No. 9, (2014), 091703.
- Gorji, S., Seddighi, M., Ariyaratne, C., Vardy, A., O'Donoghue, T., Pokrajac, D. and He, S., "A comparative study of turbulence models in a transient channel flow", *Computers & Fluids*, Vol. 89, (2014), 111-123.
- Langtry, R.B. and Menter, F.R., "Correlation-based transition modeling for unstructured parallelized computational fluid dynamics codes", *AIAA Journal*, Vol. 47, No. 12, (2009), 2894-2906.
- Malan, P., Suluksna, K. and Juntasaro, E., "Calibrating the reo transition model for commercial cfd", in Proceedings of the 47th AIAA Aerospace Sciences Meeting Including the New Horizons Forum and Aerospace Exposition., (2009), 1-20.
- Angioletti, M., Nino, E. and Ruocco, G., "Cfd turbulent modelling of jet impingement and its validation by particle image velocimetry and mass transfer measurements",

- International Journal of Thermal Sciences*, Vol. 44, No. 4, (2005), 349-356.
- Li, H.-Y., Chao, S.-M. and Tsai, G.-L., "Thermal performance measurement of heat sinks with confined impinging jet by infrared thermography", *International Journal of Heat and Mass Transfer*, Vol. 48, No. 25-26, (2005), 5386-5394.
 - El-Sheikh, H.A. and Garimella, S.V., "Heat transfer from pin-fin heat sinks under multiple impinging jets", *IEEE Transactions on Advanced Packaging*, Vol. 23, No. 1, (2000), 113-120.
 - Garimella, S.V. and Schroeder, V.P., "Local heat transfer distributions in confined multiple air jet impingement", *Journal of Electronic Packaging*, Vol. 123, No. 3, (2001), 165-172.
 - Chougule, N., Parishwad, G. and Sewatkar, C., "Numerical analysis of pin fin heat sink with a single and multi air jet impingement condition", *International Journal of Engineering and Innovative Technology*, Vol. 1, No. 3, (2012), 44-50.
 - Brignoni, L.A. and Garimella, S.V., "Experimental optimization of confined air jet impingement on a pin fin heat sink", *IEEE Transactions on Components and Packaging Technologies*, Vol. 22, No. 3, (1999), 399-404.
 - Siddique, U.M., Bhise, G.A. and Gulhane, N.P., "On numerical investigation of local nusselt distribution between flat surface and impinging air jet from straight circular nozzle and power law correlations generation", *Heat Transfer—Asian Research*, Vol. 47, No. 1, (2018), 126-149.
 - Umair, S.M. and Gulhane, N.P., "Numerical investigation of non-dimensional constant representing the occurrence of secondary peaks in the nusselt distribution curve", *International Journal of Engineering Transaction A*, Vol. 29, No. 10, (2016), 1453-1461.
 - Umair, S.M. and Gulhane, N.P., "On numerical investigation of nonuniformity in cooling characteristic for different materials of target surfaces being exposed to impingement of air jet", *International Journal of Modeling, Simulation, and Scientific Computing*, Vol. 8, No. 03, (2017), 1750024.
 - Umair, S.M. and Gulhane, N.P., "On numerical investigation of heat transfer augmentation through pin fin heat sink by laterally impinging air jet", *Procedia Engineering*, Vol. 157, (2016), 89-97.
 - Sundaram, M. and Venkatesan, M., "Heat transfer study of perforated fin under forced convection", *International Journal of Engineering*, Vol. 28, No. 10, (2015), 1500-1506.
 - Soleimani, G. and Khoshrovan-Azar, E., "A numerical study of natural convection and radiation interaction in vertical circular pin", *International Journal of Engineering*, Vol. 10, No. 3, (1997), 163-172.
 - Moffat, R.J., "Describing the uncertainties in experimental results", *Experimental Thermal and Fluid Science*, Vol. 1, No. 1, (1988), 3-17.

On Numerical Investigation of Semi-empirical Relations Representing Local Nusselt Number at Lower Nozzle-target Spacing's

S. Mohd Umair^a, N. P. Gulhane^b, A. R. A. Al-Robaian^c, S. A. Khan^d

^a MPSTME – NMIMS University, India

^b Veermata Jijabai Technological Institute, Mumbai, India

^c Qassim University, Saudi

^d Mechanical Engineering Department, Faculty of Engg., IIUM, Kuala Lumpur, Malaysia

P A P E R I N F O

چکیده

Paper history:

Received 21 November 2018

Received in revised form 19 December 2018

Accepted 03 January 2019

Keywords:

Local Nusselt Number

Prandtl Number

Nozzel

Numerical Simulation

Heat Sink

Gamma-theta Model

بررسی میزان خنک کننده با استفاده از نفوذ جت هوا، کاربرد وسیعی در بسته بندی های الکترونیکی و سیستم های متقابل حرارتی مایع در مقیاس کوچک را در بر می گیرد، در حالی که پیش بینی پروفیل Nusselt در فاصله بین فاصله بین هدف نازل یک موضوع بزرگ است. قطر محدوده متوسط Nusselt بزرگ در برابر فاصله بین هدف نازل (Z/D) نشان می دهد کاهش تدریجی در مشخصات تا $Z/d = 1$ و فراتر از آن ثابت است. هدف این مقاله پیش بینی پروفیل عدد نوسلت با استفاده از روابط نیمه تجربی است. این روابط نیمه تجربی با استفاده از تحلیل رگرسیون که بین Z/d و شماره Nusselt محلی انجام می شود، به دست آمده است. داده های مورد نیاز برای رگرسیون از طریق محاسبه به دست می آیند. شبیه سازی عددی برای پارامترهای مختلف و پارامترهای هندسی انجام می شود. روابط قانون قانون نیمه تجربی بین Z/d و Re رابطه دارد. این ها برای چهار منطقه مجزا گرمادهی (نقطه رکود، نزدیکی جت منطقه، منطقه جت دور و نزدیک منطقه دیوار) متفاوت است. همبستگی های توسعه یافته نشان دهنده میزان منفی با Z/d و مثبت با Re است. قدرت منفی Z/d و t/d به ترتیب از $0.76-0.23$ و $0.03-0.25$ در تغییر است، در حالیکه شاخص های Re در محدوده مثبت $0.76-0.4$ تغییر می نمایند.

doi: 10.5829/ije.2019.32.01a.18